

KINETIC LUMINOSITY AND COMPOSITION OF ACTIVE GALACTIC NUCLEI JETS

Kouichi Hirotani

*Max-Planck-Institut für Kernphysik, Postfach 103980, D-69029 Heidelberg, Germany
hirotani@mpi-hd.mpg.de*

ABSTRACT

We present a new method how to discriminate the matter content of parsec-scale jets of active galactic nuclei. By constraining the kinetic luminosity of a jet from the observed core size at a single very long baseline interferometry frequency, we can infer the electron density of a radio-emitting component as a function of the composition. Comparing this density with that obtained from the theory of synchrotron self-absorption, we can determine the composition. We apply this procedure to the five components in the 3C 345 jet and find that they are likely pair-plasma dominated at 11 epochs out of the total 21 epochs, provided that the bulk Lorentz factor is less than 15 throughout the jet. We also investigate the composition of the 3C 279 jet and demonstrate that its two components are likely pair-plasma dominated at three epochs out of four epochs, provided that their Doppler factors are less than 10, which are consistent with observations. The conclusions do not depend on the lower cutoff energy of radiating particles.

Subject headings: galaxies: active — quasars: individual (3C 345) — quasars: individual (3C 279) — radio continuum: galaxies

1. Introduction

The study of extragalactic jets on parsec scales is astrophysically interesting in the context of the activities of the central engines of active galactic nuclei (AGN). In particular, a determination of their matter content would be an important step in the study of jet formation, propagation and emission. There are two main candidates for their matter content: A ‘normal plasma’ consisting of (relativistic or non-relativistic) protons and relativistic electrons (Celotti and Fabian 1993; see also Gómez et al. 1993, 1994a,b for numerical simulations of shock fronts in such a jet) and a ‘pair plasma’ consisting only of relativistic electrons and positrons (e.g., Kino and Takahara 2004). Discriminating between these possibilities is crucial for understanding the physical processes occurring close to the central engine (presumably a supermassive black hole) in the nucleus.

Very long baseline interferometry (VLBI) is uniquely suited to the study of the matter content of pc-scale jets, because other observational techniques cannot image at milliarcsecond resolution and must resort to indirect means of studying the active nucleus. So far, there have been two observational approaches with VLBI to discriminate jet compositions: polarization (Wardle et al. 1998) and spectroscopic (Reynolds et al. 1996) techniques.

Wardle et al. (1998) observed the 3C 279 jet at 15 and 22 GHz. They examined the *circular* polarization ($\sim 1\%$) due to Faraday *conversion* of linear to circular polarization caused by low-energy electrons and derived that the lowest Lorentz factor, γ_{\min} , of radiating particles, should be much less than 10^2 . They also analyzed the *linear* polarization ($\sim 10\%$), which strongly limits internal Faraday *rotation* to derive that $\gamma_{\min} \gg 10^2$ must be held for a normal-plasma composition and that no constraint would be obtained for a pair-plasma composition. (Note that an equal mixture of electrons and positrons can produce Faraday conversion, but not rotation.) From these arguments, they concluded that component CW of the 3C 279 jet consists of a pair plasma with $\gamma_{\min} \ll 10^2$.

On the other hand, Reynolds et al. (1996) analyzed historical VLBI data of the M87 jet at 5 GHz (Pauliny-Toth et al. 1981) and concluded that the core is probably dominated by an e^\pm plasma. In the analysis, they utilized the standard theory of synchrotron self absorption (SSA) to constrain the magnetic field, B [G], and gave $B = 0.2$ G (line B in fig-

ure 1). They also considered the condition that the resolved core becomes optically thick for self-absorption and derived another constraint on N_e^* and B . Using the observed angular diameter of the core (0.7mas), the total core flux density (1.0 Jy) at 5 GHz, and the reported viewing angle ($30^\circ - 40^\circ$), and assuming that the spectral index is 0.5 (see end of this section), they derived $N_e^* B^2 > 2\delta_{\max}^{-1}$ in cgs unit (line C in figure 1), where δ_{\max} ($= 2$ for the M87 core) refers to the upper limit of the Doppler factor of the fluid’s bulk motion.

This condition is, however, applicable only for the VLBI observations of M87 core at epochs September 1972 and March 1973. Therefore, in order to apply the analogous method to other AGN jets or to the M87 jet at other epochs, we must derive a more general condition.

On these grounds, Hirovani et al. (1999, hereafter Paper I) generalized the condition $N_e^* B^2 > 2\delta_{\max}^{-2}$ and applied it to the 3C 279 jet on parsec scales. In that paper, they revealed that the core and components C3 and C4, of which spectra are reported, are likely dominated by a pair plasma. It is interesting to note that the same conclusion was derived by an independent method by Wardle et al. (1998) on component CW in the 3C 279.

Subsequently, Hirovani et al. (2000, hereafter Paper II) applied the same method to the 3C 345 jet. Deducing the kinetic luminosity, L_{kin} , from a reported core-position offset (Lobanov 1998), they demonstrated that components C2, C3, and C4 at epoch 1982.0, C5 at 1990.55, and C7 at four epochs are likely dominated by a pair plasma. In the present paper, we propose a new scheme to deduce the kinetic luminosity of an unresolved core and re-examine the composition of the two blazars 3C 345 and 3C 279, adding spectral information at 11 epochs for the 3C 345 jet to Paper II and 2 epochs for the 3C 279 jet to Paper I.

In the next section, we give a general expression of lines B and C in figure 1. We then describe in § 3 a new method how to infer L_{kin} from the core size observed at a single VLBI frequency; the inferred L_{kin} gives lines D₁ and D₂ in figure 1, depending on the composition. Once L_{kin} is obtained for the core by this method, we can apply it to individual jet components, assuming a constant L_{kin} along the jet. In sections 4 and 5, we examine the two blazars 3C 345 and 3C 279. In the final section, we discuss the possibility of the entrainment of the ambient matter as a jet propagates downstream.

We use a Hubble constant $H_0 = 65h$ km/s/Mpc and $q_0 = 0.5$ throughout this paper. Spectral index α is defined such that $S_\nu \propto \nu^{+\alpha}$.

2. Synchrotron self-absorption constraint in the jet region

In this paper, we model a jet component as a homogeneous sphere of angular diameter θ_d , containing a tangled magnetic field B [G] and relativistic electrons, which give a synchrotron spectrum with optically thin index α . In § 2.1, we constrain B (i.e., line B in fig. 1) for arbitrary optical thickness by the theory of synchrotron self-absorption. Once B is obtained, we can compute the electron number density N_e^* (SSA) (i.e., line C) as will be described in § 2.2 with the aid of the computed optical depth at the turnover frequency.

2.1. Magnetic field strength

The magnetic field strength, B , can be computed from the synchrotron spectrum, which is characterized by the peak frequency, ν_m , the peak flux density, S_m , and the spectral index, α , in the optically thin regime. Marscher (1983) considered a uniform spherical synchrotron source and related B with ν_m , S_m , and α for optically thin cases ($0 \geq \alpha \geq -1.0$). Later, Cohen (1985) considered a uniform slab of plasma as the synchrotron source and derived smaller values of B for the same set of (ν, S_m, α) . In this section, we express B (i.e., line B in fig. 1) in terms of (ν, S_m, α) for a uniform sphere for *arbitrary* optical thickness (i.e., for arbitrary $\alpha \leq 0$). We assume that the magnetic field is uniform and that the distribution of radiating particles are uniform in the configuration space and are isotropic and power-law (eq.[19]) in the momentum space.

For a uniform B and N_e^* , the transfer equation gives the specific intensity

$$I_\nu^* = A\nu^{*5/2} [1 - \exp(-\alpha_\nu^* x_0^*)], \quad (1)$$

where

$$A(\alpha) \equiv \left(\frac{3}{2}\right)^{-\alpha} \frac{e}{c} \frac{a(\alpha)}{C(\alpha)} \left(\frac{e}{2\pi m_e c}\right)^{-3/2} B^{-1/2}, \quad (2)$$

and x_0^* gives the physical thickness of the emitting region along the line of sight; e , m_e , and c refer to the charge on an electron, the rest mass of an electron, and the speed of light, respectively. The coefficients $a(\alpha)$ and $C(\alpha)$ are given in table 1; a quantity with

an asterisk is measured in the co-moving frame, while that without an asterisk in the observer's frame. At the distance θ away from the cloud center (fig. 2), the fractional thickness, which is Lorentz invariant, becomes

$$\frac{x_0^*}{2R^*} = \cos(\theta + \xi) = \sqrt{1 - \left[\frac{\sin \theta}{\sin(\theta_d/2)}\right]^2}, \quad (3)$$

where $R^* \cos \xi + (R^* \sin \xi / \sin \theta) \cos \theta = R^* / \sin(\theta_d/2)$ is used in the second equality; θ_d is the angular diameter of the component in the perpendicular direction of the jet propagation. Thus, the specific intensity at angle θ away from the center, becomes

$$I_\nu(\theta) = \left(\frac{\delta}{1+z}\right)^{1/2} A\nu^{5/2} \times \left\{ 1 - \exp \left[-\tau_\nu(0) \sqrt{1 - \left[\frac{\sin \theta}{\sin(\theta_d/2)}\right]^2} \right] \right\}, \quad (4)$$

where $\tau_\nu(0) \equiv \alpha_\nu^* \cdot 2R^*$ is the optical depth for $\theta = 0$ (or $b = 0$). Averaging over pitch angles of the isotropic electron power-law distribution (eq. [19]), we can write down the absorption coefficient in the co-moving frame as (Le Roux 1961, Ginzburg & Syrovatskii 1965)

$$\alpha_\nu^* = C(\alpha) r_o^2 k_e^* \frac{\nu_o}{\nu^*} \left(\frac{\nu_B}{\nu^*}\right)^{(-2\alpha+3)/2}, \quad (5)$$

where $\nu_o \equiv c/r_o \equiv c/[e^2/(m_e c^2)] = 1.063 \times 10^{14}$ GHz and $\nu_B \equiv eB/(2\pi m_e c)$. In deriving equation (4), we utilized $I_\nu/\nu^3 = I_\nu^*/\nu^{*3}$ and $\nu/\nu^* = \delta/(1+z)$, where z represents the redshift and the Doppler factor, δ , is defined by

$$\delta \equiv \frac{1}{\Gamma(1 - \beta \cos \varphi)}, \quad (6)$$

where $\Gamma \equiv 1/\sqrt{1 - \beta^2}$ is the bulk Lorentz factor of the jet component moving with velocity βc , and φ refers to the viewing angle.

Even if special relativistic effects are important, the observer find the shape to be circular. We thus integrate $I_\nu(\theta) \cos \theta$ over the emitting solid angles $2\pi \sin \theta d\theta$ in $0 \leq \theta \leq \theta_d/2$ to obtain the flux density

$$\begin{aligned} S_\nu &= 2\pi \int_0^{\theta_d/2} I_\nu(\theta) \cos \theta \sin \theta d\theta \\ &= \pi \sin^2 \left(\frac{\theta_d}{2}\right) \cdot \left(\frac{\delta}{1+z}\right)^{1/2} \end{aligned}$$

$$\times A\nu^{5/2} \int_0^1 \left(1 - e^{-\tau_\nu(0)\sqrt{1-\chi}}\right) d\chi, \quad (7)$$

where $\chi \equiv [\sin \theta / \sin(\theta_d/2)]^2$.

Differentiating equation (7) with respect to ν , and putting $dS_\nu/d\nu$ to be 0, we obtain the equation that relates $\tau_\nu(0)$ and α at the turnover frequency, ν_m ,

$$\begin{aligned} & \int_0^1 \left[1 - e^{-\tau_\nu(0)\sqrt{1-\chi}}\right] d\chi \\ &= \left(1 - \frac{2}{5}\alpha\right) \int_0^1 \tau_\nu(0)\sqrt{1-\chi} e^{-\tau_\nu(0)\sqrt{1-\chi}} d\chi \end{aligned} \quad (8)$$

We denote the solution $\tau_\nu(0)$ at $\nu = \nu_m$ as $\tau_m(0)$, which is presented as a function of α in table 1.

It is worth comparing equation (7) with that for a uniform slab of plasma with physical thickness R^* . If the slab extends over a solid angle $\pi(0.5\theta_d/\text{rad})^2$, the flux density becomes

$$S_\nu = \frac{\pi}{4} \left(\frac{\theta_d}{\text{rad}}\right)^2 \left(\frac{\delta}{1+z}\right)^{1/2} A\nu^{5/2} \left(1 - e^{-\tau_\nu(0)}\right). \quad (9)$$

The optical depth $\tau_\nu(0) = \alpha_\nu^* \cdot 2R^*$ does not depend on θ for the slab geometry. Therefore, comparing equations (7) and (9) we can define the effective optical depth, $\langle\tau_\nu\rangle$, for a uniform sphere of plasma as

$$e^{-\langle\tau_\nu\rangle} \equiv \int_0^1 e^{-\tau_\nu(0)\sqrt{1-\chi}} d\chi. \quad (10)$$

We denote $\langle\tau_\nu\rangle$ at $\nu = \nu_m$ as $\langle\tau_m\rangle$, which is presented in table 1. Note that $\langle\tau_m\rangle$ is less than $\tau_m(0)$ due to the geometrical factor $\sqrt{1-\chi}$.

Using $\tau_m(0)$, we can evaluate the peak flux density, S_m , at $\nu = \nu_m$ and inversely solve equation (7) for B . We thus obtain

$$B = 10^{-5} b(\alpha) \left(\frac{\nu_m}{\text{GHz}}\right)^5 \left(\frac{\theta_d}{\text{mas}}\right)^4 \left(\frac{S_m}{\text{Jy}}\right)^{-2} \frac{\delta}{1+z}, \quad (11)$$

where $\theta_d \ll 1$ rad is used and

$$\begin{aligned} b(\alpha) &= 3.98 \times 10^3 \left(\frac{3}{2}\right)^{-2\alpha} \left[\frac{a(\alpha)}{C(\alpha)}\right]^2 \\ &\times \left\{ \int_0^1 \left[1 - e^{-\tau_m(0)\sqrt{1-\chi}}\right] d\chi \right\}^2. \end{aligned} \quad (12)$$

The values are tabulated in table 1; they are, in fact, close to the values obtained by Cohen (1985), who

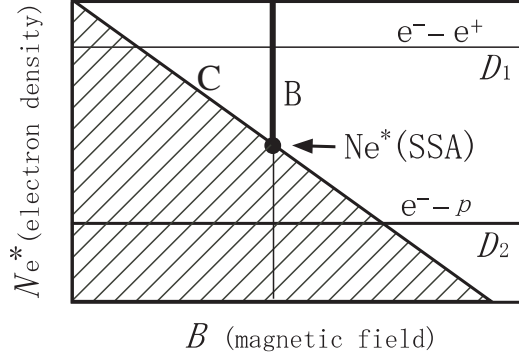


Fig. 1.— Constraints on (B, N_e^*) plane imposed by synchrotron self-absorption and total kinetic luminosity considerations (see fig. 1 in Reynolds et al. 1996). The VLBI surface brightness constraint on B gives line B, while the condition that the a jet component (or the resolved core in Reynolds et al. 1996) becomes optically thick to self-absorption gives line C. The horizontal lines are the proper densities derived from the kinetic luminosity; line D₁ and D₂ correspond to a pure pair and a pure normal plasma, respectively.

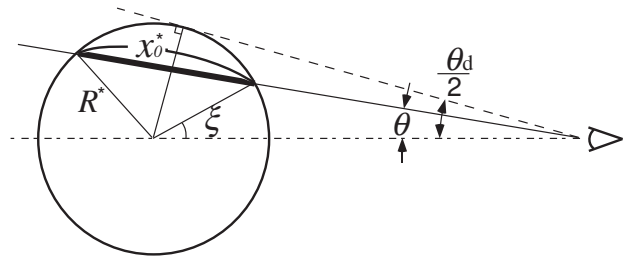


Fig. 2.— Flux emitted from a spherical cloud of radius R^* .

presented $b(\alpha)$ for a slab geometry with $-\alpha \leq 1.25$. This is because the averaged optical depth, $\langle \tau_\nu \rangle$ at $\nu = \nu_m$, for a spherical geometry becomes comparable with that for a slab geometry (Scott & Readhead 1977).

We could expand the integrant in equation (7) in the optically thin limit $\tau_m(0) \ll 1$ as

$$1 - e^{-\tau_m(0)\sqrt{1-\chi}} \approx \tau_m(0)\sqrt{1-\chi}, \quad (13)$$

to obtain $b(-0.5) = 3.34$ and $b(-1.0) = 3.85$, for example. This optically thin limit ($\tau_m \ll 1$) was considered by Marscher (1983), who gave $b(\alpha)$ for $\alpha \geq -1.0$ (i.e., for $\tau_m(0) < 1.0$).

2.2. Electron density

We next consider how to constrain N_e^* (i.e., line C in fig. 1) from the theory of synchrotron self-absorption. To examine the lower limit of N_e^* (SSA), we consider a conical jet geometry (fig.3) in this section, even though we apply the results (eqs. [22]-[24]) to individual jet components, which would be more or less spherical rather than conical. The optical depth τ for synchrotron self absorption at distance ρ from the injection point, is given by

$$\tau_\nu(\rho) = \left[\frac{\rho \sin \chi}{\sin(\varphi + \chi)} + \frac{\rho \sin \chi}{\sin(\varphi - \chi)} \right] \alpha_\nu, \quad (14)$$

where φ is the viewing angle and α_ν [1/cm] refers to the effective absorption (i.e., absorption minus stimulated emission) coefficient. For a small half opening angle ($\chi \ll 1$), this equation can be approximated as

$$\tau_\nu(\rho) = 2 \frac{\rho \sin \chi}{\sin \varphi} \alpha_\nu, \quad (15)$$

where $\chi/\sin \varphi$ denotes the projected, observed opening angle. Noting that $\rho \sin \chi$ represents the transverse thickness of the jet, we find that equation (15) holds not only for a conical geometry but also for a cylindrical one.

Since τ_ν and $\rho \sin \chi$ are Lorentz invariants, we obtain

$$\frac{\alpha_\nu}{\sin \varphi} = \frac{\alpha_\nu^*}{\sin \varphi^*}. \quad (16)$$

Since $\nu \alpha_\nu$ is also Lorentz invariant, equation (16) gives

$$\frac{\sin \varphi^*}{\sin \varphi} = \frac{\nu}{\nu^*} = \frac{\delta}{1+z}. \quad (17)$$

Combining equations (15) and (17), we obtain

$$\tau_\nu = \frac{1+z}{\delta} \frac{2\rho \sin \chi}{\sin \varphi} \alpha_\nu^* = \frac{1+z}{\delta} \frac{\theta_d}{\sin \varphi} \frac{D_L}{(1+z)^2} \alpha_\nu^*, \quad (18)$$

where $D_L/(1+z)^2$ is the angular diameter distance to the AGN; θ_d is measured in radian unit (i.e., not in milliarcsecond). Equation (18) holds for a conical geometry with an arbitrary small opening angle, including a cylindrical case.

We assume that the electron energy distribution is represented by a power-law,

$$\frac{dN_e^*}{d\gamma} = k_e^* \gamma^{2\alpha-1} \quad (\gamma_{\min} < \gamma < \gamma_{\max}), \quad (19)$$

where N_e^* refers to the proper electron number density. Integrating $dN_e^*/d\gamma$ from γ_{\min} to γ_{\max} , and assuming $\gamma_{\max} \gg \gamma_{\min}$ and $\alpha < 0$, we obtain

$$N_e^* = \frac{\gamma_{\min}^{2\alpha}}{-2\alpha} k_e^*. \quad (20)$$

The coefficient $C(\alpha)$ is given in Table 1 of Gould (1979) and also in table 1 in this paper.

Substituting equation (5) into (18), and assuming $\gamma_{\min} \ll \gamma_{\max}$, we obtain

$$N_e^* B^{-\alpha+1.5} = \frac{m_e c}{e^2} \left(\frac{e}{2\pi m_e c} \right)^{-1.5+\alpha} \frac{\tau_\nu(\alpha)}{C(\alpha)} \frac{\gamma_{\min}^{2\alpha}}{-2\alpha} \times \frac{\sin \varphi (1+z)^2}{\theta_d D_L} \left(\frac{1+z}{\delta} \right)^{-\alpha+1.5} \nu^{-\alpha+2.5}. \quad (21)$$

Evaluating ν at ν_m , and combining with equation (11), we obtain N_e^* (SSA) in cgs unit as (see also Marscher 1983 for relatively optically thin cases, $-\alpha \leq$

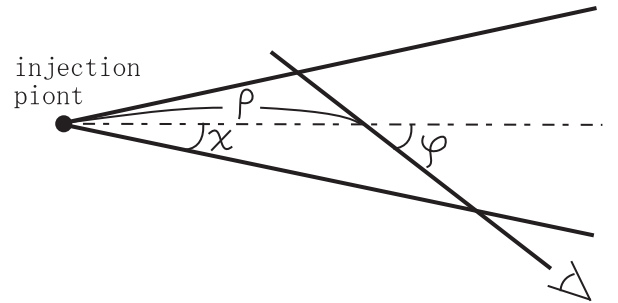


Fig. 3.— Schematic figure of a conical jet in the core region with half opening angle χ in the observer's frame.

Table 1: Table of constants

α	0	-0.25	-0.50	-0.75	-1.00	-1.25	-1.50	-1.75	-2.00
a	0.2833	0.149	0.103	0.0831	0.0740	0.0711	0.0725	0.0776	0.0865
C	1.191	1.23	1.39	1.67	2.09	2.72	3.67	5.09	7.23
$\tau_{\text{m}}(0)$	0	0.252	0.480	0.687	0.878	1.055	1.220	1.374	1.519
$\langle \tau_{\text{m}} \rangle$	0	0.167	0.314	0.445	0.564	0.672	0.770	0.862	0.946
b	0	1.66	2.36	2.34	2.08	1.78	1.51	1.27	1.08

1.0)

$$N_{\text{e}}^*(\text{SSA}) = e(\alpha) \frac{\gamma_{\text{min}}^{2\alpha} \sin \varphi}{-2\alpha} \frac{\sin \varphi}{d_{\text{A}}} \left(\frac{\theta_{\text{d}}}{\text{mas}} \right)^{4\alpha-7} \times \left(\frac{\nu_{\text{m}}}{\text{GHz}} \right)^{4\alpha-5} \left(\frac{S_{\text{m}}}{\text{Jy}} \right)^{-2\alpha+3} \left(\frac{\delta}{1+z} \right)^{2\alpha-3}, \quad (22)$$

where

$$d_{\text{A}} \equiv \frac{zq_0 + (q_0 - 1)(-1 + \sqrt{2q_0z + 1})}{h(1+z)^2q_0^2} \quad (23)$$

$$e(\alpha) \equiv 1.71 \times 10^{-9} \times [2.79 \times 10^{-8} b(\alpha)]^{\alpha-1.5} \times \frac{\tau_{\nu}}{C(\alpha)} \quad (24)$$

If the jet component is discontinuous (e.g., spherical), equation (22) gives the lower limit of $N_{\text{e}}^*(\text{SSA})$, because the path length becomes smaller than $2\rho \sin \chi / \sin \varphi$ (eq. [15]).

It looks like from equation (22) that $N_{\text{e}}^*(\text{SSA})$ depends on θ_{d} and ν_{m} very strongly. In the case of $\alpha = -0.75$, for instance, we obtain $N_{\text{e}}^*(\text{SSA}) \propto \theta_{\text{d}}^{-10} \nu_{\text{m}}^{-8}$. Nevertheless, as a radio-emitting component evolves along the jet, its θ_{d} increases due to expansion while its ν_{m} decreases due to (synchrotron+adiabatic) cooling. As a result, these two effects partially cancel each other and suppress the variations of $N_{\text{e}}^*(\text{SSA})$ along the jet.

3. Kinetic luminosity in the core region

In this section, we present a new method how to deduce the kinetic luminosity, L_{kin} , of a jet in the unresolved VLBI core from the perpendicular core size, utilizing the core-position offset among different frequencies as an intermediate variable in manipulation. Once L_{kin} is obtained for the core, we can apply it to derive lines D₁ and D₂ for individual jet components, assuming a stationary jet ejection with constant L_{kin} .

3.1. Scaling Law

Let us introduce a dimensionless variable $r \equiv \rho/r_1$ to measure ρ in parsec units, where $r_1 = 1$ pc. We

assume that the electron number density scales with r as

$$N_{\text{e}}^* = N_1 r^{-n}, \quad (25)$$

where N_1 refers to the value of N_{e}^* at $r = 1$ (i.e., at 1 pc from the core in the observer's frame). If particles are neither created nor annihilated in a conical jet, conservation of particles gives $n = 2$. In the same manner, we assume the following scaling law:

$$B = B_1 r^{-m}, \quad (26)$$

where B_1 refers to the values of B at $r = 1$. In a stationary super-fast-magnetosonic jet, the magnetic flux conservation gives $m = 1$. Note that we assume such scaling laws only in the unresolved VLBI core, not in the jet region, for which we consider $N_{\text{e}}^*(\text{SSA})$.

We further introduce the following dimensionless variables:

$$x_{\text{N}} \equiv r_1 r_{\text{o}}^2 N_1, \quad x_{\text{B}} \equiv \nu_{\text{B}1} / \nu_{\text{o}} = \frac{eB_1}{2\pi m_{\text{e}} c} \cdot \frac{1}{\nu_{\text{o}}}. \quad (27)$$

Utilizing equation (5), and rewriting k_{e}^* and ν_{B} in terms of x_{N} and x_{B} , we obtain from the left equality in equation (18)

$$\tau_{\nu} = C(\alpha) \frac{2\chi}{\sin \varphi} \frac{-2\alpha}{\gamma_{\text{min}}^{2\alpha}} \left(\frac{1+z}{\delta} \right)^{-\epsilon} \left(\frac{\nu}{\nu_{\text{o}}} \right)^{-1-\epsilon} \times r^{1-n-m\epsilon} x_{\text{N}} x_{\text{B}}^{\epsilon}, \quad (28)$$

where $\epsilon \equiv 3/2 - \alpha$. Note that both x_{N} and x_{B} should be distinguished from $N_{\text{e}}^*(\text{SSA})$ and B presented in section 2, because we are considering the core region in this section.

At a given frequency ν , the flux density will peak at the position where τ_{ν} becomes unity. Thus setting $\tau = 1$ and solving equation (28) for r , we obtain the distance from the VLBI core observed at frequency ν from the injection point as (Lobanov 1998)

$$r(\nu) = \left[x_{\text{B}}^{k_{\text{b}}} f(\alpha) \frac{\nu_{\text{o}}}{\nu} \right]^{1/k_{\text{r}}} \quad (29)$$

where

$$f(\alpha) \equiv \left[C(\alpha) \frac{2\chi}{\sin \varphi} \frac{-2\alpha}{\gamma_{\min}^{2\alpha}} \left(\frac{\delta}{1+z} \right)^\epsilon x_N \right]^{1/(\epsilon+1)} \quad (30)$$

$$k_b \equiv \frac{3-2\alpha}{5-2\alpha}, \quad (31)$$

$$k_r \equiv \frac{(3-2\alpha)m+2n-2}{5-2\alpha}. \quad (32)$$

3.2. Core-Position Offset

If we measure $r(\nu)$ at two different frequencies (say ν_a and ν_b), equation (29) gives the dimensionless, projected distance of $r(\nu_a) - r(\nu_b)$ as

$$\begin{aligned} \Delta r_{\text{proj}} &= [r(\nu_a) - r(\nu_b)] \sin \varphi \\ &= (x_B^{k_b} f \nu_o)^{1/k_r} \frac{\nu_b^{1/k_r} - \nu_a^{1/k_r}}{\nu_a^{1/k_r} - \nu_b^{1/k_r}} \sin \varphi \end{aligned} \quad (33)$$

Here, Δr_{proj} is in pc units; therefore, $r_1 \Delta r_{\text{proj}}$ represents the projected distance of the two VLBI cores (in cm, say). That is, $r_1 \Delta r_{\text{proj}}$ equals $4.85 \cdot 10^{-9} \Delta r_{\text{mas}} D_L / (1+z)^2$ in equation (4) in Lobanov (1998), where Δr_{mas} refers to the core-position difference in mas. Defining the core-position offset as

$$\Omega_{r\nu} \equiv r_1 \Delta r_{\text{proj}} \frac{\nu_a^{1/k_r} \nu_b^{1/k_r}}{\nu_b^{1/k_r} - \nu_a^{1/k_r}}, \quad (34)$$

we obtain

$$\frac{\Omega_{r\nu}}{r_1} = (x_B^{k_b} f \nu_o)^{1/k_r} \sin \varphi \quad (35)$$

Setting $\nu_b \rightarrow \infty$ in equation (33), we can express the absolute distance of the VLBI core measured at ν from the central engine as (Lobanov 1998)

$$r_{\text{core}}(\nu) = \frac{\Omega_{r\nu}}{r_1 \sin \varphi} \nu^{-1/k_r}. \quad (36)$$

To express x_B in terms of x_N and $\Omega_{r\nu}$, we solve equation (35) for x_B to obtain

$$x_B = \left(\frac{\Omega_{r\nu}}{r_1 \sin \varphi} \right)^{k_r/k_b} (f \nu_o)^{-1/k_b}. \quad (37)$$

Note that x_N is included in $f = f(\alpha)$.

We next represent x_N and x_B (or equivalently, N_1 and B_1) as a function of $\Omega_{r\nu}$. To this end, we parameterize the energy ratio between particles and the magnetic field as

$$N_e^* \gamma_{\min} m_e c^2 = K \frac{B^2}{8\pi}. \quad (38)$$

When an energy equipartition between the radiating particles and the magnetic field holds, we obtain

$$K = \frac{\gamma_{\min}}{\langle \gamma_- \rangle}, \quad (39)$$

where the averaged electron Lorentz factor, $\langle \gamma_- \rangle$ becomes

$$\begin{aligned} \langle \gamma_- \rangle &\equiv \frac{\int_{\gamma_{\min}}^{\gamma_{\max}} \gamma \cdot k_e^* \gamma^{2\alpha-1} d\gamma}{\int_{\gamma_{\min}}^{\gamma_{\max}} k_e^* \gamma^{2\alpha-1} d\gamma} \\ &= \frac{2\alpha}{2\alpha+1} \gamma_{\min} \frac{(\gamma_{\max}/\gamma_{\min})^{2\alpha+1} - 1}{(\gamma_{\max}/\gamma_{\min})^{2\alpha} - 1}. \end{aligned} \quad (40)$$

for $\alpha < 0$. We assume a rough energy equipartition holds and adopt

$$K \sim \frac{2\alpha+1}{2\alpha} \frac{(\gamma_{\max}/\gamma_{\min})^{2\alpha} - 1}{(\gamma_{\max}/\gamma_{\min})^{2\alpha+1} - 1}. \quad (41)$$

In the limit $\alpha \rightarrow -0.5$, the right-hand side tends to $1/\ln(\gamma_{\max}/\gamma_{\min})$, which is 0.1 if $\gamma_{\max} = 10^{4.34} \gamma_{\min}$, for instance. Note that we assume a rough energy equipartition in the core and not in the jet.

In this paper, we assume that K/γ_{\min} is constant for r . Then, equation (38) requires $n = 2m$. Substituting $N_e^* = N_1 r^{-2m}$ and $B = B_1 r^{-m}$ into equation (38), and replacing N_1 and B_1 with x_N and x_B , we obtain

$$x_N = \frac{\pi}{2} \frac{K}{\gamma_{\min}} \frac{r_1}{r_o} x_B^2 \quad (42)$$

Combining equations (37) and (42), we obtain

$$\begin{aligned} x_B &= \left[\frac{1}{\nu_o} \left(\frac{\Omega_{r\nu}}{r_1 \sin \varphi} \right)^{k_r} \right]^{(5-2\alpha)/(7-2\alpha)} \\ &\times \left[\pi C(\alpha) \frac{\chi}{\sin \varphi} \frac{K}{\gamma_{\min}} \frac{r_1}{r_o} \frac{-2\alpha}{\gamma_{\min}^{2\alpha}} \left(\frac{\delta}{1+z} \right)^\epsilon \right]^{-2/(7-2\alpha)} \end{aligned} \quad (43)$$

For ordinary values of $\alpha (< 0)$, x_B decreases with increasing K , as expected. The particle number density, x_N , can be readily computed from equation (42).

3.3. Kinetic Luminosity

When the jet has a cross section πR_\perp^2 at a certain position, L_{kin} and N_e^* are related by

$$L_{\text{kin}} = \pi R_\perp^2 \beta c \Gamma N_e^* (\Gamma-1) (\langle \gamma_- \rangle m_e c^2 + \langle \gamma_+ \rangle m_+ c^2), \quad (44)$$

where $\langle \gamma_+ \rangle$ refers to the averaged Lorentz factors of positively charged particles, and m_+ designates the mass of the positive charge.

Assuming that the particle number is conserved, we find that $\pi R_\perp^2 \beta c \cdot \Gamma N_e^*$ is constant along a stationary jet. Thus, provided that $\Gamma \gg 1$ holds, $R_\perp^2 N_e^*$ can be replaced as

$$R_\perp^2 N_e^* = \frac{\Gamma_1}{\Gamma} (r_1 \chi_1)^2 N_1 = \frac{\Gamma_1}{\Gamma} \chi_1^2 \frac{r_1}{r_o^2} x_N, \quad (45)$$

where Γ_1 and χ_1 refer to Γ and χ at 1 pc. Substituting equation (45) into (44), we obtain

$$\begin{aligned} L_{\text{kin}} &= C_{\text{kin}} K \frac{r_1^2}{r_o^3} \beta \Gamma_1 (\Gamma - 1) \left(\frac{\chi_1}{\chi} \right)^2 \\ &\times \left[\frac{\chi}{\nu_o} \left(\frac{\Omega_{r\nu}}{r_1 \sin \varphi} \right)^{k_r} \right]^{2(5-2\alpha)/(7-2\alpha)} \\ &\times \left[\frac{\pi C(\alpha)}{\sin \varphi} \frac{K}{\gamma_{\text{min}}} \frac{r_1}{r_o} \frac{-2\alpha}{\gamma_{\text{min}}^{2\alpha}} \left(\frac{\delta}{1+z} \right)^{3/2-\alpha} \right]^{-4/(7-2\alpha)}; \quad (46) \end{aligned}$$

we adopt $C_{\text{kin}} = \pi^2 \langle \gamma_- \rangle m_e c^3 / \gamma_{\text{min}}$ for a pair plasma, while $C_{\text{kin}} = \pi^2 \langle \gamma_+ \rangle m_p c^3 / (2\gamma_{\text{min}})$ for a normal plasma, where m_p refers to the rest mass of a proton. Equation (46) holds not only for a conical jet but also for a general jet with $\Gamma \gg 1$ provided that the particle number is conserved and that $n = 2m$ holds. It should be noted that γ_{min} takes different values between a pair and a normal plasma.

3.4. Jet Opening Angle

Let us now consider the half opening angle of the jet, and further reduce the expression of L_{kin} . As noted in § 3.3, we obtain

$$\chi = \frac{R_\perp}{\rho} = \frac{0.5 \theta_{\text{d,core}}(\nu)}{\rho} \frac{D_L}{(1+z)^2} \quad (47)$$

for a conical geometry, where $\theta_{\text{d,core}}(\nu)$ is the angular diameter of the VLBI core at a frequency ν in the perpendicular direction to the jet-propagation direction on the projected plane (i.e., a VLBI map). The luminosity distance is given by

$$D_L = 4.61 \times 10^9 h^{-1} r_1 \frac{q_0 z + (q_0 - 1)(-1 + \sqrt{2q_0 z + 1})}{q_0^2}. \quad (48)$$

On the other hand, equation (36) gives

$$\rho = r_{\text{core}} r_1 = \frac{\Omega_{r\nu}}{\sin \varphi} \nu^{-1/k_r} \quad (49)$$

Substituting equations (49), (48) into (47), we obtain

$$\begin{aligned} \frac{1}{\nu_o} \frac{\chi \Omega_{r\nu}}{r_1 \sin \varphi} &= 11.1 h^{-1} \frac{q_0 z + (q_0 - 1)(-1 + \sqrt{2q_0 z + 1})}{q_0^2 (1+z)^2} \\ &\times \left(\frac{\theta_{\text{d,core}}}{\text{mas}} \right) \frac{\nu^{1/k_r}}{\nu_o}. \quad (50) \end{aligned}$$

Since $m = 1$ is consistent with the theory of magnetohydrodynamics, we will adopt $k_r = 1$ in the rest of this paper. Then, it follows that the factor containing $\chi \Omega_{r\nu} / \sin \varphi$ in equation (46) can be simply expressed in terms of $\theta_{\text{d,core}}(\nu)$. That is, to evaluate L_{kin} , we do not have to stop on the way at the computation of $\Omega_{r\nu}$, which requires more than two VLBI frequencies. We only need the VLBI-core size at a single frequency, $\theta_{\text{d,core}}(\nu)$, in addition to Γ , φ , α , γ_{min} , z , K , and C_{kin} . If we have to examine χ , we additionally need $\Omega_{r\nu}$. The information of the composition is included in C_{kin} . In the present paper, we assume $\Gamma \chi^2 = \Gamma_1 \chi_1^2$.

If k_r deviates from unity, we have to independently examine χ and $\Omega_{r\nu}$. In another word, we need at least two VLBI frequencies (e.g., 2 and 8 GHz) to measure the core-position offset in order to constrain L_{kin} , even if we know the value of k_r by some means.

To constrain Γ in equation (46), let us briefly consider how to obtain its lower bound. If the apparent velocity of a radio-emitting component, $\beta_{\text{app}} = \beta \sin \varphi / (1 - \beta \cos \varphi)$, reflects the fluid velocity, the lower bound can be obtained by $\Gamma_{\text{min}} \equiv \sqrt{\beta_{\text{app}}^2 + 1}$. On the other hand, the upper bound of Γ is not easily constrained; thus, we must consider it source by source, using observations at different photon energies (e.g., X-rays) if necessary.

3.5. Electron density deduced from kinetic luminosity

Once L_{kin} is known by the method described above or by some other methods, we can compute the electron number density as a function of the composition. We assume that the L_{kin} deduced for the core can be applied for the individual jet components. Then, solving equation (44), which holds not only in the core but also in the jet, for N_e^* , and utilizing $R_\perp = (\theta_{\text{d}}/2) D_L / (1+z)^2$, we obtain for a normal plasma

$$N_e^*(\text{nml}) = 5.93 \times 10^{-2} h^2 \frac{L_{46}}{\Gamma(\Gamma - 1)} \left(\frac{\theta_{\text{d}}}{\text{mas}} \right)^{-2}$$

$$\times \left[\frac{q_0^2(1+z)^2}{zq_0 + (q_0 - 1)(-1 + \sqrt{2q_0z + 1})} \right]^2 \\ \times \frac{1}{\langle \gamma_+ \rangle} \frac{1}{1 + \langle \gamma_- \rangle m_e/m_p} \text{ cm}^{-3}, \quad (51)$$

where $L_{46} = L_{\text{kin}}/(10^{46} \text{ ergs s}^{-1})$. If $N_e^*(\text{nml})$ becomes less than the electron density deduced independently from the theory of synchrotron self-absorption (SSA), the possibility of a normal plasma dominance can be ruled out.

It is worth comparing $N_e^*(\text{nml})$ with $N_e^*(\text{pair})$, the particle density in a pure pair plasma. If we compute L_{kin} by using equation (46) and (50), we obtain the following ratio

$$\frac{N_e^*(\text{pair})}{N_e^*(\text{nml})} = \frac{L_{\text{kin}}(\text{pair})}{L_{\text{kin}}(\text{nml})} \frac{m_p c^2 + \langle \gamma_-(\text{nml}) \rangle m_e c^2}{2 \langle \gamma_-(\text{pair}) \rangle m_e c^2} \\ = \frac{\gamma_{\text{min}}(\text{nml})}{\gamma_{\text{min}}(\text{pair})}, \quad (52)$$

where $\gamma_{\text{min}}(\text{pair})$ and $\gamma_{\text{min}}(\text{nml})$ refer to γ_{min} in a pair and a normal plasma, respectively; $\langle \gamma_-(\text{pair}) \rangle$ and $\langle \gamma_-(\text{nml}) \rangle$ refer to the averaged Lorentz factor of electrons in a pair and a normal plasma, respectively. Therefore, if $\gamma_{\text{min}}(\text{pair})$ is comparable to $\gamma_{\text{min}}(\text{nml}) \sim 100$, there is little difference between $N_e^*(\text{pair})$ and $N_e^*(\text{nml})$.

3.6. Summary of the Method

Let us summarize the main points that have been made in §§ 2 and 3.

- (1) We can compute the magnetic field strength (i.e., line B in fig. 1) from the surface brightness condition.
- (2) We can also constrain the proper electron density and the magnetic field strength (i.e., line C) from the synchrotron self-absorption constraint.
- (3) Combining (1) and (2), we obtain the electron density, $N_e^*(\text{SSA})$, for each radio-emitting component.
- (4) Observing the core size, $\theta_{\text{d,core}}(\nu)$, at a single frequency, ν , and substituting equation (50) into equation (46), we obtain the kinetic luminosity, L_{kin} .
- (5) Assuming a normal-plasma dominance, we obtain the proper electron density, $N_e^*(\text{nml})$ (i.e., line D₂) from L_{kin} by equation (51).
- (6) If $N_e^*(\text{nml}) \ll N_e^*(\text{SSA})$ holds, we can rule out the possibility of a normal-plasma dominance and that of a pair-plasma dominance with $\gamma_{\text{min}} \sim 100$ or greater. That is, $N_e^*(\text{nml}) \ll N_e^*(\text{SSA})$ indicates the dominance of a pair plasma with $\gamma_{\text{min}} \ll 100$.

4. Application to the 3C 345 Jet

Let us apply the method described in the previous sections to the radio-emitting components in the 3C 345 jet and investigate the composition. This quasar ($z = 0.595$; Hewitt & Burbidge 1993) is one of the best studied objects showing structural and spectral variabilities on parsec scales around the compact unresolved core (for a review, see e.g., Zensus 1997). At this redshift, 1 mas corresponds to $5.85h^{-1}$ pc, and 1 mas yr^{-1} to $\beta_{\text{app}} = 30.3h^{-1}$.

4.1. Kinetic luminosity

To deduce L_{kin} , we first consider $\theta_{\text{d,core}}\nu/\nu_0$, where $k_r = 1$ is adopted in equation (50). From the reported core size at 22.2 GHz at 6 epochs by Zensus et al. (1995), at 5 epochs by Unwin et al. (1997), and at 3 epochs by Ros et al. (2000), we can deduce the averaged core size, $\theta_{\text{d,core}}$, as 0.296 mas (fig. 4); here, we evaluate the core size with $1.8\sqrt{ab}$ for the latter three epochs, where a and b refer to the major and minor axes at the FWHM of the elliptical Gaussian presented in Ros et al. (2000). From $\theta_{\text{d,core}} = 0.296$ mas, we obtain $\theta_{\text{d,core}}\nu/\nu_0 = 6.18 \times 10^{-14}$ as the averaged value over the 14 epochs at 22 GHz. In the same manner, we obtain the following averaged values at different frequencies: $\theta_{\text{d,core}} = 0.258$ mas and $\theta_{\text{d,core}}\nu/\nu_0 = 3.64 \times 10^{-14}$ over 3 epochs at 15 GHz (Ros et al. 2000); $\theta_{\text{d,core}} = 0.436$ mas and $\theta_{\text{d,core}}\nu/\nu_0 = 4.38 \times 10^{-14}$ over 7 epochs at 10.7 GHz (1 epoch from Unwin et al. 1994; 4 epochs from Zensus et al. 1995; 2 epochs from Gabuzda et al. 1999); $\theta_{\text{d,core}} = 0.343$ mas and $\theta_{\text{d,core}}\nu/\nu_0 = 2.71 \times 10^{-14}$ over 7 epochs at 8.4 GHz (1 epoch from Unwin et al. 1994; 3 epochs from Zensus et al. 1995; 3 epochs from Ros et al. 2000); $\theta_{\text{d,core}} = 0.423$ mas and $\theta_{\text{d,core}}\nu/\nu_0 = 1.98 \times 10^{-14}$ over 11 epochs at 5.0 GHz (4 epochs from Brown et al. 1994; 1 epoch from Unwin et al. 1994; 3 epochs from Zensus et al. 1995; 3 epochs from Ros et al. 2000). Taking a weighted average of $\theta_{\text{d,core}}\nu/\nu_0$ over the 42 epochs at the different 5 frequencies, we obtain

$$\frac{\theta_{\text{d,core}}\nu}{\nu_0} = 4.01 \times 10^{-14}. \quad (53)$$

We next consider the spectral index that reflects the energy distribution of the power-law electrons in the core. From infrared to optical observations (J,H,K,L bands from Sitko et al. 1982; J,H,K bands from Neugebauer et al. 1982; K band from Impey et

al. 1982; IRAS 12, 25, 60, 100 microns from Moshir et al. 1990), we obtain

$$\alpha = -1.15 \quad (54)$$

for the core. This value is consistent with that adopted by Zensus et al. (1995).

Using equations (53) and (54), we obtain from equation (50)

$$\left(\frac{1}{\nu_0} \frac{\chi \Omega_{r\nu}}{r_1 \sin \varphi} \right)^{2(5-2\alpha)/(7-2\alpha)} = 4.97 \times 10^{-21} h^{-1.57}. \quad (55)$$

Moreover, $\alpha = -1.15$ gives

$$\begin{aligned} & \left[\pi C(\alpha) \frac{-2\alpha K}{\gamma_{\min}^{2\alpha+1}} \frac{r_1}{r_0} \right]^{-4/(7-2\alpha)} \\ &= 1.31 \times 10^{-14} K^{-0.43} \gamma_{\min}^{-0.56}. \end{aligned} \quad (56)$$

We thus obtain

$$\begin{aligned} L_{\text{kin}} &= 4.68 \times 10^{45} h^{-1.57} \langle \gamma_+ \rangle \left(\frac{\gamma_{\min}}{100} \right)^{-1.56} K^{0.57} \\ &\times \Gamma(\Gamma - 1) \left[\frac{1}{\sin \varphi} \left(\frac{\delta}{1+z} \right)^{2.65} \right]^{-0.43} \text{ ergs s}^{-1} \end{aligned} \quad (57)$$

for a normal plasma, that is, $C_{\text{kin}} = \pi^2 \langle \gamma_+ \rangle m_p c^3 / (2\gamma_{\min})$ in equation (46). Note that the factor $\langle \gamma_+ \rangle$ cancels out when we compute $N_e^*(\text{nml})$ by equation (51) and hence does not affect the conclusions on the matter content in the present paper. However, to examine the absolute kinetic luminosity of a normal-plasma-dominated jet, we have to independently know $\langle \gamma_+ \rangle$, because we can constrain only the electron density by SSA theory.

4.2. Kinematics near the core

To constrain L_{kin} further, we must consider the kinematics of the core and evaluate Γ and φ . In the case of the 3C 345 jet, components are found to be ‘accelerated’ as they propagate away from the core. For example, for component C4, $\beta_{\text{app}} h < 8$ held when the distance from the core was less than 1 mas (Zensus et al. 1995); however, it looked to be ‘accelerated’ from this distance (or epoch 1986.0) and attained $\beta_{\text{app}} h \sim 45$ at epoch 1992.5 (Lobanov & Zensus 1994). It is, however, unlikely that the fluid bulk Lorentz factor increases so much during the propagation. If β_{app} reflected the fluid bulk motion of C4, the bulk Lorentz factor, Γ , had to be at least 45 until 1992.5. Then

$\beta_{\text{app}} \sim 6$ during 1981-1985 indicates that the viewing angle should be less than 0.05° , which is probably much less than the opening angle. Analogous ‘acceleration’ was reported also for C3 (Zensus et al. 1995) and C7 (Unwin et al. 1997).

On these grounds, we consider the apparent ‘acceleration’ of the components in their later stage of propagation on VLBI scales are due to geometrical effects such as ‘scissors effects’ (Hardee & Norman 1989; Fraix-Burnet 1990), which might be created at the intersection of a pair of shock waves. Such shock waves may be produced, for example, by the interaction between relativistic pair-plasma beam and the ambient, non-relativistic normal-plasma wind (Sol, Pelletier & Asséo 1989; Pelletier & Roland 1989; Pelletier & Sol 1992; Despringre & Fraix-Burnet 1997; Pelletier & Marcowith 1998). In their two-fluid model, the pair beam could be destructed at a certain distance from the core on VLBI scales due to the generation of Langmuir waves.

Then, how should we constrain Γ and φ for the 3C 345 jet? In this paper, we assume that the radio-emitting components before their rapid acceleration represent (or mimic) the fluid bulk motion. Under this assumption, Steffen et al. (1995) fitted the motions of C4 (during 1980-1986) and C5 (during 1983-1989) when the components are within 2 mas from the core by a helical model. They found $\Gamma = 5.8$ for C4 and 4.6 for C5 with $\varphi = 6.8^\circ$, assuming $h = 1.54$ (i.e., $H_0 = 100 \text{ km/s/Mpc}$). These Lorentz factors will be ~ 9 and ~ 7 for C4 and C5, respectively, if $h = 1$ (i.e., $H_0 = 65 \text{ km/s/Mpc}$). Subsequently, Qian et al. (1996) investigated the intrinsic evolution of C4 under the kinematics of $\Gamma = 5.6$ and $\varphi = 2^\circ - 8^\circ$, assuming $h = 1.54$; the range of viewing angles is in good agreement with $\varphi = 2^\circ$ (for C4) – 4° (for C2) at 1982.0 obtained by Zensus et al. (1995), who used a larger value of $\Gamma = 10$ under $h = 1.54$, which corresponds to $\Gamma \sim 15$ for $h = 1$.

Unless a substantial deceleration takes place, the assumption of a constant Lorentz factor is justified as the first order of approximation. In the last part of § 4.3, we will examine the case when the Lorentz factor is different from this assumed value and consider how the conclusion of the composition depends on Γ . Close to the core, we adopt $\varphi = 2^\circ$, because the viewing angle is suggested to decrease with decreasing distance from the core (Zensus et al. 1995; Unwin et al. 1997). If φ is less than 2° in the core, L_{kin} , and hence $N_e^*(\text{nml})$ further decreases; that is, the normal-

plasma dominance can be further ruled out. In short, we apply $K = 0.1$, $\Gamma = 15$ and $\varphi = 2^\circ$ in equation (57). Assuming a normal-plasma dominance, we adopt $\gamma_{\min} = 10^2$ for electron energy distribution.

4.3. Composition of individual components

We can now investigate the composition of the radio-emitting components in the 3C 345 jet, using their spectral information. We assume that the jet is neither accelerated nor decelerated and apply the Lorentz factor obtained for the (unresolved) core to all the (resolved) jet components. To compute $N_e^*(\text{SSA})$, we further need φ for each component at each epoch. (Note that $\varphi = 2^\circ$ is assumed for the core, not for the components.) For this purpose, we assume that β_{app} reflects the fluid motion if $\beta_{\text{app}} < \sqrt{\Gamma^2 - 1}$ and that φ is fixed after β_{app} exceeds $\sqrt{\Gamma^2 - 1}$. That is, we compute φ from

$$\tan \varphi = \begin{cases} \frac{2\beta_{\text{app}}}{\beta_{\text{app}}^2 + \delta^2 - 1} & \text{if } \beta_{\text{app}} < \sqrt{\Gamma^2 - 1} \\ \frac{1}{\sqrt{\Gamma^2 - 1}} & \text{if } \beta_{\text{app}} > \sqrt{\Gamma^2 - 1} \end{cases} \quad (58)$$

The constancy of φ when $\beta_{\text{app}} > \sqrt{\Gamma^2 - 1} = 15.0$ could be justified by the helical model of Steffen et al. (1995), who revealed that the viewing angle does not vary significantly after the component propagates a certain distance (about 1 mas in the cases of components C4 and C5) from the core. As we will see in table 2 (later in this subsection), φ increases with increasing distance from the core and do not deviate significantly from the assumed value for the core (2 degree)."

The synchrotron self-absorption spectra of individual components are reported in several papers. They were first reported in Unwin et al. (1994), who presented (ν_m, S_m, α) and θ_d (or ξ in their notation) of components C4 and C5 at epoch 1990.7. Subsequently, Zensus et al. (1995) gave (ν_m, S_m, α) , θ_d , and $\beta_{\text{app}}h$ for C2, C3, and C4 at 1982.0. However, the errors are given only for θ_d ; therefore, we evaluate the errors of the output parameters, δ , φ , B , $N_e^*(\text{nml})$, and $N_e^*(\text{nml})/N_e^*(\text{SSA})$, using the errors in θ_d alone for C2, C3, and C4 at 1982.0. Later, Unwin et al. (1997) presented (ν_m, S_m, α) , θ_d , and $\beta_{\text{app}}h$ of C5 (at 1990.55) and C7 (at 1992.05, 1992.67, 1993.19, and 1993.55). More recently, Lobanov and Zensus (1999) presented a comprehensive data of (ν_m, S_m, α) of C3, C4, and C5 at various epochs. We utilize

$\theta_d = 0.114 + 0.0658(\text{epoch} - 1979.50)$ for C4 (Qian et al. 1996), $\theta_d = 0.114 + 0.0645(\text{epoch} - 1980.00)$ for C5, which is obtained from the data given in Zensus et al. (1995) and Unwin et al. (1997), and $\theta_d = 0.09 + 0.45(\rho \sin \varphi / \text{mas})$ for C3 (Biretta et al. 1986), where $\rho \sin \varphi$ refers to the projected distance from the core.

The results for individual components at various epochs are given in table 2 for $K = 0.1$. It follows that the ratio, $N_e^*(\text{nml})/N_e^*(\text{SSA})$ becomes less than 1 if the magnetic field is an acceptable strength, (e.g., $B < 100\text{mG}$). For C4, we cannot rule out the possibility of a normal-plasma dominance at epochs 1985.8 and 1988.2. Nevertheless, at these two epochs, unnatural input parameters ($\alpha = -0.2$ at epoch 1985.8 and $S_m = 0.8$ Jy at epoch 1988.2) give too large B ($> 380\text{mG}$) for a moderate δ (< 30). If we instead interpolated S_m and α at epochs 1985.8 and 1988.2 from those at epochs 1983.4 and 1990.7, we would obtain reasonable values $B = 70$ mG and $N_e^*(\text{nml})/N_e^*(\text{SSA}) = 0.28$ at epoch 1985.8, and $B = 50$ mG and $N_e^*(\text{nml})/N_e^*(\text{SSA}) = 0.046$ at epoch 1988.2. On the other hand, C5 at 1984.2 gives unusual value $N_e^*(\text{SSA}) = 3.7 \times 10^5 \text{cm}^{-3}$. It is due to the unnaturally small value of ν_m ($= 2.5$ GHz) in the early stage of its evolution.

For an assumed Lorentz factor $\Gamma = 15$ throughout the jet, we present the results of $N_e^*(\text{nml})/N_e^*(\text{SSA})$ as a function of the projected distance $\rho \sin \varphi$ in figure 5. The horizontal solid line represents $N_e^* = N_e^*(\text{nml})$. It should be noted that $\langle \gamma_- \rangle \sim 10^3$ holds in equation (51) for a normal plasma. Thus, the solid line gives the upper limit of $N_e^*(\text{nml})/N_e^*(\text{SSA})$. What has been noticed is that the possibility of a normal-plasma dominance can be ruled out if $N_e^*(\text{nml})/N_e^*(\text{SSA}) \ll 1$ holds. There is also depicted a horizontal dashed line representing $0.01N_e^*(\text{nml})/N_e^*(\text{SSA}) \approx N_e^*(\text{pair})/N_e^*(\text{SSA})$ (see eq. [52]). If the ratio appears near the dashed line, it indicates that the homogeneous component is pair dominated. The horizontal dotted line corresponds to $(2/1836)N_e^*(\text{nml})/N_e^*(\text{SSA})$. If the ratio appears under this line, it means that L_{kin} is underestimated for that particular component. If ν_m resides within the observed frequency range, the point and error bar is indicated by thick pen, whereas if ν_m resides outside of the observed frequency range (i.e., if ν_m is extrapolated and hence contains a large error together with S_m) it is indicated by thin one. The two points appearing above the solid line correspond to C4 at 1985.8 and 1988.2, which have the unnat-

ural input parameters as discussed in the foregoing paragraph.

It follows from the figure that the upper bound of the 68%-error bars for the 11 epochs appear below 0.1, and hence that the jet is likely pair-plasma dominated, provided $\Gamma \sim 15$. (C5 at 1984.2 is not counted in the 11 epochs, because it gives too small $N_e^*(\text{nml})/N_e^*(\text{SSA})$ value.) For a smaller Γ , $N_e^*(\text{nml})/N_e^*(\text{SSA})$ further decreases. However, in this case, the ratio appears lower than the dotted line, indicating that L_{kin} is underestimated for those jet components with $\Gamma < 15$, or that $\langle \gamma_+ \rangle \gg 1$ holds for a normal plasma composition. The ratio shows no evidence of evolution as a function of the projected distance, $\rho \sin \varphi$, under the assumption of a constant Γ .

It is noteworthy that $N_e^*(\text{nml})/N_e^*(\text{SSA})$ is proportional to $(\gamma_{\text{min}}/100)^{-2\alpha-1.56}$ for the spectral index of -1.15 for the core. Therefore, for a typical spectral index $\alpha \sim -0.75$ for the jet components, the dependence on γ_{min} virtually vanishes. That is, the conclusion does not depend on the assumed value of $\gamma_{\text{min}} \sim 100$ for a normal plasma.

If we assume instead $\Gamma = 20$ (rather than $\Gamma = 15$) and $\varphi = 2^\circ$, we obtain the following kinetic luminosity

$$L_{\text{kin}} = 1.3 \times 10^{46} h^{-1.57} \langle \gamma_+ \rangle \left(\frac{\gamma_{\text{min}}}{100} \right)^{-1.56} K^{0.56} \text{ergs s}^{-1}. \quad (59)$$

Evaluating the viewing angles of individual components by equation (58) with $\Gamma = 20$, we can compute $N_e^*(\text{nml})/N_e^*(\text{SSA})$ as presented in figure 6. It follows from this figure that we cannot rule out the possibility of a normal-plasma dominance for such large Lorentz factors. The greater Γ we assume, the greater becomes $N_e^*(\text{nml})/N_e^*(\text{SSA})$.

5. Application to the 3C 279 Jet

Let us next consider the 3C 279 jet. This quasar ($z = 0.538$) was the first source found to show superluminal motion (Cotton et al. 1979; Unwin et al. 1989). At this redshift, 1 mas yr^{-1} corresponds to $\beta_{\text{app}} = 28.2h^{-1}$.

5.1. Kinetic luminosity

In the same manner as in 3C 345 case, we first consider $\theta_{\text{d,core}} \nu / \nu_0$. Since the turnover frequency of the core is reported to be about 13 GHz (Unwin et al. 1989), we measure $\theta_{\text{d,core}}$ at $\nu \leq 10.7$

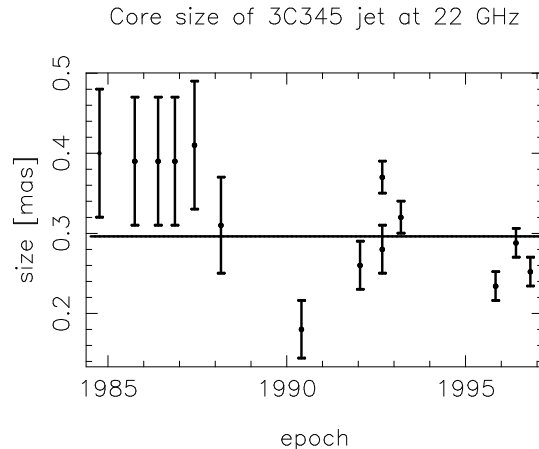


Fig. 4.— Angular core size of the 3C 345 core at 22.2 GHz. The horizontal line represents the best fit value.

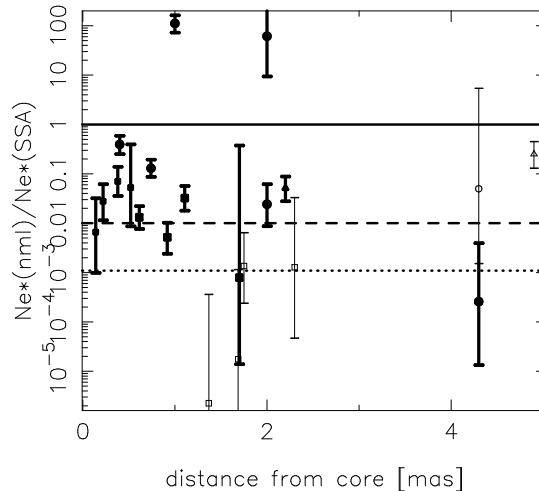


Fig. 5.— The ratio $N_e^*(\text{nml})/N_e^*(\text{SSA})$ as a function of the distance from the core. Above the solid, horizontal line, the dominance of a normal plasma is allowed. $\Gamma = 15$ is assumed.

GHz (i.e., optically thick frequency range). At 10.7 GHz, $\theta_{\text{d,core}}$ is reported to be 0.79 mas from five-epoch observations by Unwin et al. (1989), and 0.61 mas from three-epoch observations by Carrara et al. (1993). With one-epoch VSOP (VLBI Space Observatory Programme) observation, $\theta_{\text{d,core}} = 1.8 \times 0.28$ mas and $\theta_{\text{d,core}} = 1.8 \times 1.95$ mas were obtained at 4.8 GHz and 1.6 GHz, respectively (Piner et al. 2000). As the weighted mean over the 10 epochs, we obtain

$$\frac{\theta_{\text{d,core}}\nu}{\nu_0} = 6.6 \times 10^{-14}, \quad (60)$$

which leads to

$$\begin{aligned} \frac{1}{\nu_0} \frac{\chi\Omega_{r\nu}}{r_1 \sin \varphi} &= 2.8h^{-1} \left(\frac{\theta_{\text{d,core}}}{\text{mas}} \right) \frac{\nu}{\nu_0} \\ &= 3.7 \times 10^{-13}. \end{aligned} \quad (61)$$

We next consider the spectral index of the core in the optical thin frequencies. From mm to IRAS (90-150 GHz and 270-370 GHz) observations, Grandi et al. (1996) reported

$$\alpha = -1.2. \quad (62)$$

Adopting this value as the spectral index that reflects the energy distribution of the power-law electrons in the core, we obtain

$$\left(\frac{1}{\nu_0} \frac{\chi\Omega_{r\nu}}{r_1 \sin \varphi} \right)^{2(5-2\alpha)/(7-2\alpha)} = 2.7 \times 10^{-20} h^{-1.57}. \quad (63)$$

and

$$\begin{aligned} &\left[\pi C(\alpha) \frac{-2\alpha K}{\gamma_{\text{min}}^{2\alpha+1}} \frac{r_1}{r_0} \right]^{-4/(7-2\alpha)} \\ &= 1.81 \times 10^{-14} K^{-0.43} \gamma_{\text{min}}^{-0.56}. \end{aligned} \quad (64)$$

If we assume a normal plasma dominance, we obtain

$$\begin{aligned} L_{\text{kin}} &= 3.0 \times 10^{46} h^{-1.57} \left(\frac{\gamma_{\text{min}}}{100} \right)^{-1.56} K^{0.57} \\ &\times \Gamma(\Gamma - 1) \left[\frac{1}{\sin \varphi} \left(\frac{\delta}{1+z} \right)^{2.7} \right]^{-0.43} \text{ ergs s}^{-1}. \end{aligned} \quad (65)$$

5.2. Kinematics near the core

We now consider Γ and φ near to the core to constrain L_{kin} further. The apparent superluminal velocities of the components in the 3C 279 jet do not show

the evidence of acceleration and are roughly constant during the propagation. For example, Carrara et al. (1993) presented $\beta_{\text{app}} = 4.51h^{-1}$ for C3 during 1981 and 1990 over 15 epochs at 5, 11, and 22 GHz and $\beta_{\text{app}} = 4.23h^{-1}$ for C4 during 1985 and 1990 over 15 epochs at 11 and 22 GHz. We thus assume that the apparent motion of the components represent the fluid bulk motion and that both Γ and φ are kept constant throughout this straight jet. Since β_{app} does not differ very much between C3 and C4, we adopt $\beta_{\text{app}} = 4.51$ as the common value and apply the same Γ and φ for these two components. The errors incurred by the difference in β_{app} are small.

The lower bound of Γ can be obtained as $\Gamma > \sqrt{\beta_{\text{app}}^2 + 1} = 4.61$. The upper bound of Γ , on the other hand, can be obtained by the upper bound of δ for a given $\beta_{\text{app}} = 4.51$. In general, the upper bound of δ is difficult to infer. In the case of 3C 279, however, it is reasonable to suppose that a substantial fraction of the X-ray flux in the flaring state is produced via synchrotron self Compton (SSC) process. Therefore, the Doppler factors ~ 3.9 (Mattox et al. 1993) and ~ 5 (Henri et al. 1993) derived for the 1991 flare, and ~ 6.3 (Wehrle et al. 1998) for the X-ray flare in 1996, give good estimates. We thus consider that δ does not greatly exceed 10 for the 3C 279 jet. Imposing $\delta < 10$, we obtain $\Gamma < 6.06$ from $\beta_{\text{app}} = 4.61$. Combining with the lower bound, we can constrain the Lorentz factor in the range $4.6 < \Gamma < 6.1$.

As case 1, we adopt the smallest bulk Lorentz factor, $\Gamma = 4.61$, which results in $\varphi = 12.5^\circ$ and $\delta = 4.6$ for $\beta_{\text{app}} = 4.51$. It is worth comparing this δ with that measured in the quiescent state; Unwin derived $\delta = 3.6_{-1.6}^{+4.0}$ so that the calculated X-ray flux may agree with the observation. Moreover, from the RXTE observation in the 0.1-2.0 keV band during 1996.06 and 1996.11, Lawson and M^cHardy (1998) obtained $2\mu\text{Jy}$ in the quiescent state during 1996.49–1996.54 from 16-epoch observations. Applying this X-ray flux density to the spectral information (ν_{m} , S_{m} , α) and θ_{d} (table 3) for component C4 at epochs 1987.40 and 1989.26 and component C3 at 1984.05, we obtain $\delta > 1.9$, > 4.0 , and > 3.3 , respectively. Therefore, we can regard that the value of $\delta = 4.6$ are consistent with the X-ray observations. In this case, equation (65) gives

$$L_{\text{kin}} = 7.2 \times 10^{46} K^{0.57} \langle \gamma_{+} \rangle \left(\frac{\gamma_{\text{min}}}{100} \right)^{-1.6} h^{-1.6} \text{ ergs s}^{-1} \text{ (case 1)}. \quad (66)$$

As case 2, we adopt a large Lorentz factor of

$\Gamma = 6.0$. In this case, $\beta_{\text{app}} = 4.51$ gives $\delta = 9.8$ and $\varphi = 4.45^\circ$. There is, in fact, another branch of solution that gives smaller Doppler factor of 2.2; however, this solution gives too large $N_e^*(\text{SSA})$'s ($\sim 10^5 \text{cm}^{-3}$). We thus consider only the solution giving $\delta = 9.8$ as case 2, which results in

$$L_{\text{kin}} = 3.5 \times 10^{46} K^{0.57} \langle \gamma_+ \rangle \left(\frac{\gamma_{\text{min}}}{100} \right)^{-1.6} h^{-1.6} \text{ ergs s}^{-1} \text{ (case 2)}. \quad (67)$$

We will examine these two cases in the next subsection.

5.3. Composition of individual components

For the jet component C3, Unwin et al. (1989) presented $\nu_m = 6.8$ GHz, $S_m = 9.4$ Jy, $\alpha = -1.0$, and $\theta_d = 0.95$ mas at epoch 1983.1 (table 3). It was also reported in their paper that the flux densities were 5.13 ± 0.14 Jy at 5.0 GHz (at epoch 1984.25), 4.49 ± 0.17 Jy at 10.7 GHz (1984.10), and 2.58 ± 0.18 Jy at 22.2 GHz (1984.09) for C3. We model-fit the three-frequency data by the function

$$S_\nu = A_1 [1 - \exp(-A_2 \nu^{\alpha-2.5})]. \quad (68)$$

Assuming $\alpha = -1.0$, we obtain $\nu_m = 6.6$ GHz and $S_m = 5.9$ Jy as the best fit at epoch 1984.10.

For C4, Carrara et al. (1993) presented $\nu_m \sim 11$ GHz, $S_m \sim 4.3$ Jy, $\alpha = -0.9$, and $\theta_d \sim 0.6$ mas from their 1989-1990 maps at 5, 11, and 22 GHz. At epoch 1987.4, we use the flux density of 1.43 ± 0.17 Jy at 22 GHz (Carrara et al. 1993) and that of 3.95 ± 0.20 Jy at 5 GHz (Gabuzda et al. 1999). We extrapolate the flux density at 11 GHz from those at 1988.17, 1989.26, and 1990.17 presented in Carrara et al. (1993) to obtain 3.60 ± 0.20 Jy. Assuming $\alpha = -0.9$, we can model fit the three-frequency data to obtain $\nu_m = 6.4$ GHz and $S_m = 4.4$ Jy. At this epoch (1987.4), component C4 is located about 1 mas from the core; therefore, the angular size vs. distance relation (Carrara et al. 1993) gives $\theta_d \sim 0.6$ mas. The input parameters for C3 and C4 at these 4 epochs are summarized in table 3.

In case 1 (see § 5.2), we obtain $N_e^*(\text{SSA}) = 4.3 \times 10^3$ and 3.0×10^4 , for C3 at 1983.1 and 1984.10, and 8.0×10^3 and 6.4×10^1 for C4 at 1987.4 and 1989.26, respectively. These large values of $N_e^*(\text{SSA})$ in the first three epochs result in such (un-physically) small values of $N_e^*(\text{nml})/N_e^*(\text{SSA})$ as 1.4×10^{-4} , 2.9×10^{-5} , and 1.9×10^{-4} . Since even a pair-plasma dominance should be ruled out for $N_e^*(\text{nml})/N_e^*(\text{SSA}) \ll 100$ (see

eq. [52]), we consider that the value of $\delta (= 4.6)$ is underestimated.

We next examine case 2, in which a larger Doppler factor ($= 9.8$) is adopted. In this case, we obtain reasonable values of B and $N_e^*(\text{SSA})$ as presented in table 3. It follows that the ratio $N_e^*(\text{nml})/N_e^*(\text{SSA})$ becomes 4.3×10^{-3} and 8.7×10^{-3} , for C3 at 1983.1 and 1984.10, and 5.0×10^{-3} and 0.62 for C4 at 1987.4 and 1989.26, respectively. If δ exceeds 10 (or equivalently, if Γ exceeds 6), the density ratio for C4 at 1989.26 becomes close to unity; therefore, we cannot rule out the possibility of a normal-plasma dominance for such large Doppler factors.

On these grounds, we can conclude that the jet components are dominated by a pair plasma with $\gamma_{\text{min}} \ll 100$, provided that $\delta < 10$ holds, in the first three epochs. For the last epoch (1989.26), the 68%-error bar of $N_e^*(\text{nml})/N_e^*(\text{SSA})$ appears above 0.1; thus, we cannot rule out the possibility of a normal-plasma dominance. If δ is as small as 5, not only a normal-plasma dominance but also a pair-plasma dominance should be ruled out for the first three epochs. Thus, we consider δ is greater than 5 for the 3C 379 jet.

6. Discussion

In summary, we derived a general scheme to infer the kinetic luminosity of an AGN jet using a core size observed at a single VLBI frequency. The kinetic luminosity gives an electron density as a function of the composition of the jet. If the density deduced under the assumption of a normal-plasma dominance becomes much less than that obtained independently from the theory of synchrotron self-absorption, we can exclude the possibility of a normal-plasma dominance. Applying this method to the 3C 345 jet, we found that components C2, C3, C4, C5, and C7 are dominated by a pair plasma with $\gamma_{\text{min}} \ll 100$ at 11 epochs out of the total 21 epochs examined, provided that $\Gamma < 15$ holds throughout the jet. We also investigated the 3C 279 jet and found that components C3 and C4 are dominated by a pair plasma with $\gamma_{\text{min}} \ll 100$ at three epochs out of the four epochs examined, provided that $\delta < 10$.

It is noteworthy that the kinetic luminosity computed from equations (46) and (50) has, in fact, weak dependence on the composition. Substituting C_{kin} for

a pair and a normal plasma, we obtain

$$\begin{aligned} \frac{L_{\text{kin}}(\text{pair})}{L_{\text{kin}}(\text{nml})} &= \frac{m_e \langle \gamma_{-}(\text{pair}) \rangle / \gamma_{\text{min}}(\text{pair})}{m_p / 2 \gamma_{\text{min}}(\text{nml})} \\ &= \frac{1}{9.18} \frac{\langle \gamma_{-}(\text{pair}) \rangle}{\gamma_{\text{min}}(\text{pair})} \frac{\gamma_{\text{min}}(\text{nml})}{100}. \end{aligned} \quad (69)$$

It follows from equation (40) that $\langle \gamma_{-}(\text{pair}) \rangle / \gamma_{\text{min}}(\text{pair}) \sim 3$ holds for $\alpha = -0.75$, for instance. Thus, we obtain comparable kinetic luminosities irrespectively of the composition assumed, if we evaluate them by the method described in § 3.

Let us examine the assumption of $K \sim 0.1$. For a typical value of $\alpha = -0.75$, we obtain $(\langle \gamma_{-} \rangle / \gamma_{\text{min}})K = (\delta_{\text{eq}}/\delta)^{17/2}$, where δ_{eq} refers to the ‘‘equipartition Doppler factor’’ defined by (Readhead 1994)

$$\begin{aligned} \delta_{\text{eq}} &\equiv \left\{ 10^{-3-6\alpha} F(\alpha)^{34} d(z)^2 \right. \\ &\quad \times \left. (1+z)^{17-2\alpha} \nu_m^{-35-2\alpha} S_m^{16} \theta_d^{-34} \right\}^{1/(13-2\alpha)}, \end{aligned} \quad (70)$$

where

$$d(z) \equiv \frac{0.65h}{q_0 z + (q_0 - 1)(-1 + \sqrt{2q_0 z + 1})}, \quad (71)$$

and $F(\alpha)$ is given in Scott and Readhead (1977); ν_m , S_m , and θ_d are measured in GHz, Jy, and mas, respectively. Therefore, we can expect a rough energy equipartition between the radiating particles and the magnetic field if δ_{eq} is close the δ derived independently.

Substituting the input parameters presented in table 2, we can compute δ_{eq} 's for the 3C 345 jet. The computed δ_{eq} ranges between 1.1 and 67 except for component C5 at 1984.2, which gives $\delta_{\text{eq}} = 736$ due to unnaturally small ν_m . If we singled out this epoch, we would obtain $\delta_{\text{eq}} = 23 \pm 9$. The resultant magnetic field strength, $B = 6.7 \pm 6.4$ mG, is reasonable. For the 3C 279 jet, we obtain $\delta_{\text{eq}} = 9.5 \pm 1.5$ and 12 ± 8 mG for the four epochs examined.

Since $\delta_{\text{eq}} = 23 \pm 9$ for 3C 345 is consistent with those presented in table 2 and since $\delta_{\text{eq}} = 9.5 \pm 1.5$ for 3C 279 is consistent with those in table 3, we can expect a rough energy equipartition in these two blazer jets. However, it may be worth noting that the energy density of the radiating particles dominates that of the magnetic field if δ becomes much smaller than δ_{eq} . Such a case ($\delta = 4 \sim 12$) was discussed by Unwin et al. (1992; 1994; 1997) for the 3C 345 jet, assuming that a significant fraction of the X-rays was emitted

via SSC from the radio-emitting components considered.

We finally discuss the composition variation along the jet. In the application to the two blazers, we assumed constant Lorentz factors (Γ) throughout the jet. However, Γ may in general decrease with increasing distance from the central engine. If the decrease of Γ is caused by an entrainment of the ambient matter (e.g., disk wind) consisting of a normal plasma, it follows from equation (51) that $N_e^*(\text{nml})$ and hence $N_e^*(\text{nml})/N_e^*(\text{SSA})$ increases at the place where the entrainment occurs. (Note that the kinetic luminosity will not decrease due to an entrainment in a stationary jet.) Therefore, the change of composition from a pair plasma into a normal plasma along the jet may be found by the method described in this paper.

To study further the change of the composition, we need detailed spectral information (ν_m , S_m , α) of individual components along the jet. To constrain the spectral turnover accurately, we must model-fit and decompose the VLBI images from high to low frequencies; in another word, spatial resolution at low frequencies is crucial. Therefore, simultaneous observations with ground telescopes at higher frequencies and with space+ground telescopes at lower frequencies are essential for this study.

Acknowledgments

The author wishes to express his gratitude to Drs. S. Kameno, A. P. Lobanov and J. Kirk for valuable comments.

REFERENCES

- Biretta, J. A., Moore, R. L., & Cohen, M. H. 1986, ApJ 308, 93
- Brown, L. F., Roberts, D. H., and Wardle, J. F. C. 1994, ApJ 437, 108
- Celotti, A., Fabian, C. 1993, MNRAS 264, 228
- Cohen, M. H. 1985, in Extragalactic Energetic sources, Indian Academy of Sciences, Bangalore, p. 1
- Despringre, V. & Fraix-Burnet, D. 1997, AA 320, 26.
- Fraix-Burnet, D. 1990, A& A 227, 1
- Gabuzda, D. C., Mioduszewski, A. J., Roberts, D. H., Wardle, J. F. C. 1999, MNRAS 303, 515

- Ginzburg, V. L., Syrovatskii, S. I. 1965, *Ann. Rev. Astron. Astrophys.* 3, 297
- Gómez, J. L., Alberdi, A., & Marcaide, J. M. 1993, *AA* 274, 55
- Gómez, J. L., Alberdi, A., & Marcaide, J. M. 1994a, *AA* 284, 51
- Gómez, J. L., Alberdi, A., & Marcaide, J. M. 1994b, *AA* 292, 33
- Ghisellini, G., Padovani, P., Celotti, A., & Maraschi, L. 1992 *MNRAS* 258, 776
- Gould 1979, *AA* 76, 306
- Hardee, P. E., Norman, M. L. 1989, *ApJ* 342, 680
- Henri, G., Pelletier, G., Roland, J. 1993, *ApJ* 404, L41
- Hewitt, A., Burbidge, G. 1993, *ApJs* 87, 451
- Hirovani, K., Iguchi, S., Kimura, M., & Wajima, K. 1999, *PASJ* 51, 263 (Paper I)
- Hirovani, K., Iguchi, S., Kimura, M., & Wajima, K. 2000, *ApJ* 545, in press (Paper II)
- Impey, C. D., Brand, P. W. J. L., Wolstencroft, R. D., and Williams, P. M. 1982, *MNRAS* 200, 19
- Lawson, A. J., McHardy, I. M. 1998, *MNRAS* 300, 1023
- Le Roux, E. 1961, *Ann. Astrophys.* 24, 71
- Lobanov, A. P., Zensus, J. A. 1994, in *Compact Extragalactic Radio Sources*, ed. Zensus, J. A., Kellermann, K. I., National Radio Astronomy Observatory Workshop No. 23, p. 157
- Lobanov, A. P. 1998, *AA* 330, 79
- Lobanov, A. P., Zensus, J. A. 1999, *ApJ* 521, 509
- Marscher, A. P. 1983, *ApJ* 264, 296
- Moshir, M., Kopan, G., Conrow, T., McCallon, H., Hacking, P., Gregorich, D., Rohrbach, G., Melnyk, M., Rice, W., Fullmer, L. et al. 1990, in *Infrared Astronomical Satellite Catalogs, the faint source catalog*, ver. 2.0
- Mattox, J. R., Bertsch, D. L., Chiang, J. et al. 1993, *ApJ* 410, 609
- Neugebauer, G., Soifer, B. T., Matthews, K., Margon, B., Chanan, G. A. *AJ* 1982, 87, 1639
- Pauliny-Toth I. I. K., Preuss E., Witzel A., Graham D., Kellermann I. I., Romang B. 1981, *AJ* 86, 371
- Pelletier, G., & Marcowith, I. 1998, *ApJ* 502, 598
- Pelletier, G., Roland, J. 1989, *A & A* 224, 24
- Pelletier, G., & Sol, H. 1992, *MNRAS* 254, 635
- Piner, B. G., Edwards, P. G., Wehrle, A. E., Hirabayashi, H., Lovell, J. E. J., and Unwin, S. C. 2000, *ApJ* 537, 91
- Qian, S. J., Krichbaum, T. P., Zensus, J. A., Steffen, W., Witzel, A. 1996, *A & A* 308, 395
- Readhead 1994, *ApJ* 426, 51
- Reynolds, C. S., Fabian, A. C., Celotti, A., & Rees, M. J. 1996 *MNRAS* 283, 873
- Ros, E., Zensus, J. A., Lobanov, A. P. 2000, *A & A* 354, 55
- Scott, M. A., Readhead, A. C. S. 1977, *MNRAS* 180, 539
- Sitko, M. L. Stein, W. A., Zhang, Y. X., Wisniewski, W. Z. 1982, *ApJ* 259, 486
- Sol, H. Pelletier, G., & Asséo, E. 1989, *MNRAS* 237, 411
- Steffen, W., Zensus, J. A., Krichbaum, T. P., Witzel, A., Qian, S. J. 1995, *A & A* 302, 335
- Unwin, S. C., Cohen, M. H., Biretta, J. A., Hodges, M. W., and Zensus, J. A. 1989, *ApJ* 340, 117
- Unwin, S. C., Wehrle, A. E. 1992, *ApJ* 398, 74
- Unwin, S. C., Wehrle, A. E., Urry C. M., Gilmore, D. M., Barton, E. J., Kjerulf, B. C., Zensus, J. A., and Rabaca, C. R. 1994, *ApJ* 432, 103
- Unwin, S. C., Wehrle, A. E., Lobanov, A. P., Zensus, J. A., & Madejski, G. M. 1997, *ApJ* 480, 596
- Wardle, J. F. C., Homan, D. C., Ojha, R., Roberts, D. H. *Nature* 395, 457
- Wehrle, A. E., Pian E., Urry, C. M., et al. 1998, *ApJ* 497, 178

Zensus, J. A., Cohen, M. H., & Unwin, S. C. 1995,
ApJ 443, 35

Zensus, J. A. 1997, Ann. Rev. Astron. Astrophys. 35,
607

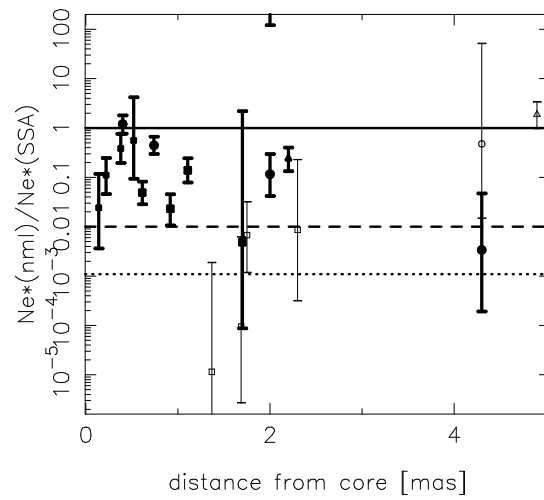


Fig. 6.— The same figure as figure 3, but the different Lorentz factor $\Gamma = 20$ is adopted.

Table 2: Input parameters and the results for the 3C 345 jet when $\Gamma = 15$.

epoch	$\rho \sin \varphi^\dagger$ mas	$\beta_{\text{app}} h^\dagger$	ν_m^\dagger GHz	S_m^\dagger Jy	α^\dagger	θ_d^\dagger mas	δ	φ deg	B mG	$N_e^*(\text{SSA})$ cm^{-3}	$N_e^*(\text{nml})/N_e^*(\text{SSA})$ (68 % errors)
						component	C2				
1982.00 ^a	4.9	12.9	1.5	2.0	-0.60	$2.15 \pm .18$	22.5	2.2	1.4E1	6.2E-4	2.5E-1 (1.3E-1, 4.5E-1)
						component	C3				
1981.50 ^b	2.0	8.7	2.7 ± 0.3	2.4 ± 0.2	-0.80	1.00	27.2	1.2	9.7E0	2.9E-2	2.4E-2 (8.6E-3, 6.1E-2)
1992.00 ^a	2.2	9.2	2.6	2.1	-0.70	$0.97 \pm .07$	26.8	1.3	9.5E0	1.5E-2	5.1E-2 (2.8E-2, 8.7E-2)
						component	C4				
1982.00 ^a	0.4	6.2	14.6	7.6	-0.30	$0.29 \pm .02$	28.6	.82	2.7E1	2.2E-2	3.9E-1 (2.5E-1, 5.8E-1)
1983.40 ^b	0.7	6.0	11.6 ± 0.4	7.5 ± 0.6	-0.50	0.37	28.7	.81	2.9E1	4.0E-2	1.3E-1 (8.6E-2, 1.9E-1)
1985.80 ^b	1.0	7.9	9.4 ± 0.6	1.9 ± 0.1	-0.20	0.53	27.7	1.1	3.9E2	2.3E-5	1.1E2 (7.2E1, 1.6E2)
1988.20 ^a	2.0	14.2	6.5 ± 1.4	0.8 ± 0.1	-0.60	0.69	19.7	2.8	1.2E3	2.4E-5	6.1E1 (9.5E0, 2.8E2)
1990.70 ^c	4.3	14.0	2.0 ± 0.5	2.0 ± 0.5	$-0.75 \pm .15$	0.85	20.3	2.6	1.2E0	3.8E0	2.6E-4 (1.4E-5, 3.8E-3)
1992.50 ^b	4.3	13.4	2.7 ± 1.6	1.6 ± 0.1	-0.70	0.97	21.7	2.4	1.6E1	1.5E-2	5.0E-2 (1.5E-3, 5.5E0)
						component	C5				
1982.20 ^b	0.3	5.0	2.5 ± 0.4	4.9 ± 1.1	-0.80	0.27	29.1	.67	9.0E-3	3.7E+5	2.6E-8 (4.8E-9, 1.4E-7)
1985.80 ^b	0.6	6.4	6.0 ± 0.3	3.3 ± 0.3	-0.60	0.37	28.5	.86	5.7E0	4.0E-1	1.3E-2 (7.6E-3, 2.2E-2)
1987.30 ^b	0.9	7.5	7.0 ± 0.6	5.1 ± 0.2	-0.80	0.47	28.0	1.0	1.3E1	6.2E-1	5.2E-3 (2.4E-3, 1.0E-2)
1988.20 ^b	1.1	8.0	7.5 ± 0.4	5.6 ± 0.5	-0.70	0.53	27.6	1.1	2.4E1	7.9E-2	3.2E-2 (1.8E-2, 5.6E-2)
1989.20 ^b	1.4	8.6	2.5 ± 1.4	4.7 ± 0.6	-0.90	0.59	27.2	1.2	2.0E-1	9.1E2	2.3E-6 (6.1E-8, 3.5E-4)
1990.30 ^b	1.7	9.3	2.5 ± 1.2	3.6 ± 0.1	-0.90	0.66	26.7	1.3	5.2E-1	9.3E1	1.8E-5 (5.0E-7, 1.1E-3)
1990.55 ^d	1.8	9.5	2.7 ± 0.5	3.2 ± 0.5	-0.75	0.80	26.5	1.4	2.2E0	8.2E-1	1.4E-3 (2.4E-4, 6.5E-3)
1990.70 ^c	1.7	11.3	2.7 ± 1.5	3.2 ± 0.9	$-0.75 \pm .15$	$0.80 \pm .20$	24.8	1.7	2.1E0	1.4E0	7.9E-4 (1.5E-5, 4.2E-1)
1992.50 ^b	2.3	11.2	2.2 ± 0.8	1.5 ± 0.3	-0.90	0.81	24.9	1.7	3.4E0	8.5E-1	1.3E-3 (4.7E-5, 3.3E-2)
						component	C7				
1992.05 ^d	0.1	2.8	12.8 ± 0.5	4.6 ± 0.5	-0.75	$0.20 \pm .04$	29.7	.36	1.1E1	2.7E0	6.6E-3 (1.0E-3, 3.1E-2)
1992.67 ^d	0.2	6.0	12.5 ± 1.0	7.0 ± 0.5	-0.75	$0.35 \pm .02$	28.7	.80	3.9E1	2.1E-1	2.8E-2 (1.1E-2, 6.1E-2)
1993.19 ^d	0.4	10.5	11.6 ± 0.5	5.1 ± 0.5	-0.75	$0.41 \pm .02$	25.7	1.6	8.6E1	6.0E-2	7.0E-2 (3.5E-2, 1.3E-1)
1993.55 ^d	0.5	14.5	11.0 ± 1.5	3.1 ± 1.0	-0.75	$0.38 \pm .02$	20.9	2.6	1.1E2	8.8E-2	5.3E-2 (8.9E-3, 4.1E-1)

[†] For the input parameters, 1σ errors are presented if they are given in the literature.

^a Input parameters are cited from Zensus et al. (1995).

^b Input parameters are cited from Lobanov and Zensus (1999).

^c Input parameters are cited from Unwin et al. (1994).

^d Input parameters are cited from Unwin et al. (1997).

Table 3: Input parameters and the results for the 3C 279 jet in case 2.

epoch	$\rho \sin \varphi$ mas	$\beta_{\text{app}} h$	ν_m GHz	S_m Jy	α	θ_d mas	δ	φ deg	B mG	$N_e^*(\text{SSA})$ cm^{-3}	$N_e^*(\text{nml})/N_e^*(\text{SSA})$ (68 % errors)	
						component	C3					
1983.10 ^a	1.4	4.5	6.8	9.4	-1.0	0.95	9.8	4.5	1.8E1	3.5E1	4.3E-3 (3.6E-3, 5.0E-3)	
1984.10 ^b	1.4	4.5	6.5	8.9	-1.0	0.80	9.8	4.5	8.2E0	2.5E2	8.7E-4 (7.3E-4, 1.0E-3)	
						component	C4					
1987.40 ^b	1.0	4.2	6.4	4.4	-0.9	0.60	9.8	4.5	9.8E0	7.7E1	5.0E-3 (4.1E-3, 5.7E-3)	
1989.26 ^c	1.2	4.2	11.0	4.3	-0.9	0.60	9.8	4.5	1.6E2	6.2E-1	6.2E-1 (2.9E-1, 1.3E0)	

^a Input parameters are cited from Unwin et al. (1989).

^b Input parameters are computed in this paper (see text).

^c Input parameters are cited from Carrara et al. (1993).